ACS Catalysis

Research Article

pubs.acs.org/acscatalysis

Nitrogen-Doped Graphene Nanosheets as Metal-Free Catalysts for Aerobic Selective Oxidation of Benzylic Alcohols

Jinlin Long,* Xiuqiang Xie, Jie Xu, Quan Gu, Liming Chen, and Xuxu Wang*

Research Institute of Photocatalysis, Fujian Provincial Key Laboratory of Photocatalysis, State Key Laboratory Breeding Base, Fuzhou University, Fuzhou 350002, People's Republic of China

Supporting Information

ABSTRACT: This work demonstrates the molecular engineering of active sites on a graphene scaffold. It was found that the N-doped graphene nanosheets prepared by a high-temperature nitridation procedure represent a novel chemical function of efficiently catalyzing aerobic alcohol oxidation. Among three types of nitrogen species doped into the graphene lattice—pyridinic N, pyrrolic N, and graphitic N—the graphitic sp^2 N species were established to be catalytically active centers for the aerobic oxidation reaction based on good linear correlation with the activity results. Kinetic analysis showed that the N-doped graphene-catalyzed aerobic alcohol oxidation proceeds via a Langmuir−Hinshelwood pathway and has moderate activation energy (56.1 ± 3.5 kJ·mol^{-1} for the benzyl alcohol oxidation) close to that (51.4 kJ·mol^{-1}) proceeding on the catalyst Ru/Al_2O_3 reported in literature. An adduct mechanism was proposed to be different remarkably from that occurring on the noble metal catalyst. The possible formation of a sp^2 N−O_2 adduct transition state, which can oxidize alcohols directly to aldehydes without any byproduct, including H_2O_2 and carboxylic acids, may be a key element step. Our results advance graphene chemistry and open a window to study the graphitic sp^2 nitrogen catalysis.

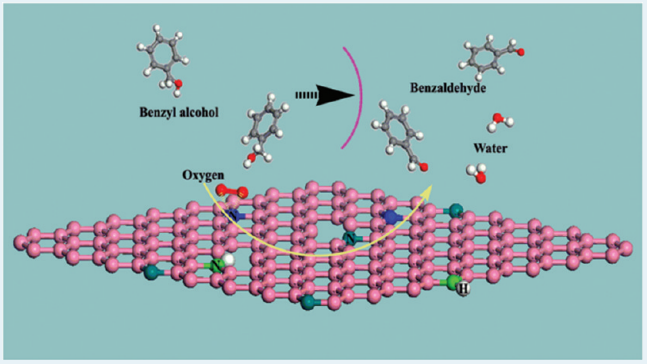

KEYWORDS: *graphene, nitrogen doping, nonmetal catalysis, selective oxidation, alcohols, aldehydes*

The selective oxidation of alcohols to their corresponding aldehydes is one of crucially important organic reactions in the synthesis of fine chemicals and intermediates.[1−3] Over the last several decades, such a functional group transformation was generally performed by several chemical processes involving either the use of organic nitrogen-containing compounds and organometallic compounds as catalysts[1,4−10] or the use of stoichiometric quantities of inorganic oxidant, notably chromium(VI) reagents.[11] These traditional homogeneous chemical processes are contradictory to the principles of green chemistry and sustainable development from both economic and environmental viewpoints, and consequently, substantial effort has been devoted to development of efficient and environmentally benign heterogeneous processes for the oxidation reaction to meet the increasingly stringent ecological standards.[12−14] In a search for cleaner green technologies, there is a definite need for alcohol oxidation that uses water as a solvent, molecular oxygen as an oxidant, and recoverable solid materials as catalysts so as to reduce secondary contamination and facilitate a continuous large-scale operation.

Although the advantages of the aerobic oxidation process proceeding in water are evident, reports on the subject are still scarce. The majority of work remains focus on both organocatalytic systems[15−19] and organometallic complex-catalyzed systems.[1,20,21] Only a few solid catalysts, such as octahedral molecular sieves;[22,23] Ru/Al_2O_3;[24] RuO_2-supported zeolites;[25] and Pd, Pt, and Au nanoparticles,[26−33] have been found to be catalytically active for aerobic oxidation of alcohols without the aid of TEMPO, but their efficiency is unsatisfactory, as indicated by the low TOF value. Recently, significant progress in this field has been made by Hutchings et al.,[34] who developed a solvent-free catalytic oxidation system using Au−Pd/TiO_2 solid catalysts. This work enkindles intense interest in the design of desirable solid catalysts for the selective oxidation of primary alcohols.

Many efficient heterogeneous systems based on active noble metals, including Pt, Pd, Au, Ru, and their alloys, have been reported[35] and received increasing attention. However, an intrinsically pivotal issue that the selective oxidation of alcohols to aldehydes by molecular oxygen commonly is accompanied by the formation of a large amount of H_2O_2 as a byproduct seems to be unavoidable in these noble-metal-catalyzed systems and some TEMPO-catalyzed systems. H_2O_2 can further react with oxygen-containing products, leading to selectivity loss.[34] How to avoid deep oxidation during selective oxidation has puzzled chemists for a long time and, thus, stimulated us to

Received: January 18, 2012
Revised: March 12, 2012
Published: March 13, 2012

explore a novel nonmetal-catalytzed system for realizing the atom-economic reaction of R−OH + (1/2)O_2 = RHO + H_2O.

Earlier studies have proved that the nitroxyl radical in efficient TEMPO-catalyzed systems is the catalyst for the oxidation of primary alcohols.[36,37] This inspires us to design and construct a new metal-free solid catalyst with unique catalytic performance analogous to the nitroxyl radical by transplanting the active N component into an inert support with a doping strategy instead of simple supporting of TEMPO.[38−41]

Graphene is such a perfect scaffold for molecular engineering of the N active sites owing to its excellent conductivity, high surface area, and two-dimensional flat honeycomb lattice. Many studies have shown that doping heteroatoms can effectively modulate the electrical properties and surface physicochemical features of graphene and introduce a considerable amount of defects into a lattice.[42−45] As a result, the introduction of heteroatoms often brings about some new functions. For example, the electrocatalytical reduction of oxygen has been recently explored as a promising application of N-doped graphene in fuel cells.[46−50]

Recently, significant progress has been made in the carbocatalysis of carbon materials. Su[51−53] reported an oxidative dehydrogenation and hydrodation reaction catalyzed by carbon nanotubes. More recently, Bielawski and co-workers[54−60] have shown a comprehensive study on the chemical function of graphene oxide, which was able to catalyze several new chemical processes, including C−H oxidation, autotandem oxidation−hydration−aldol coupling reaction, oxidation of thiols and sulfides, and dehydrative polymerization. Herein, we demonstrate another new chemical function of N-doped graphene. It was found that the multilayer graphene nanosheets doped substitutionally by N heteroatoms can efficiently catalyze aerobic selective oxidation of primary alcohols via an adduct mechanism under mild conditions. Dioxygen molecules may be activated by the N-graphene to possibly form an sp^2 N−O_2 adduct transition state, which can oxidize alcohols to directly aldehydes without any byproduct, including H_2O_2 and carboxylic acids.

RESULTS AND DISCUSSION

Synthesis and Characterization of N-Doped Graphene Nanosheets. Thermal annealing of graphite oxide (GO) in ammonia reported by Dai et al.[61] is a facile route and, thus, used to obtain gram-scale NG materials in this work. In our preparation procedure for the NG materials, natural flake graphite as the starting materials was first oxidized to GO by a modified Hummers method reported in the litertaure,[62] and then three N-doped graphene samples (denoted as NG-T, where T means nitridation temperature) were prepared by a postnitridation of GO in flowing NH_3 atmosphere at a temperature range of 1073−1273 K. Undoped graphene was prepared by a high-temperature exfoliation of GO in He atmosphere at 1073 K, without introducing NH_3 in the feedstock. It is also referred to generally as reduced GO in the literature.[63] All of the as-prepared samples were characterized by transmission electron microscopy (TEM), X-ray powder diffraction (XRD), visible Raman spectroscopy, and atomic force microscopy (AFM).

Figure 1 shows XRD patterns of the three NG-T samples and the undoped graphene sample. GO represents one main reflection centered at 10.9°, corresponding to a *c*-axis interlayer spacing of 0.81 nm (see Figure S1 in the Supporting Information). It indicates that graphite is oxidized completely. After GO was annealed in He atmosphere at 1073 K for 10 h, it shows three weak and broad diffraction lines at ∼15.5° (*d* = 0.57 nm), 22.6° (*d* = 0.39 nm), and 26.6° (*d* = 0.34 nm) in the patterns, followed by the complete disappearance of the characteristic peak of GO at ∼10.9°. It suggests that GO cannot be completely and uniformly exfoliated by the interlayer expansion along the *c*-axis direction at such a temperature, leading to the formation of graphene nanosheets with a range of thickness. But after being annealed in NH_3 atmosphere above 1073 K for 10 h, the (002) reflection of GO is retained, and the characteristic peak at ∼10.9° disappears completely. Especially for the NG-800 sample, a considerable amount of N-graphene sheets was not completely exfoliated to single-layer along the *c*-axis direction, as indicated by the two broad peaks at ∼15.5° and 22.6°. Comparison of the intensity of the two broad peaks finds that increasing the annealing temperature can more effective in exfoliating the expanded graphene sheets.

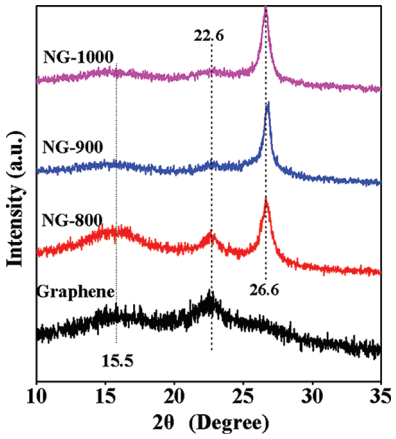

Figure 1. XRD patterns of the as-made NG-T and graphene samples.

The morphology and structure of these as-made NG-T samples and the graphene sample were studied further by TEM, HRTEM, and EDX analysis. As shown in Figure 2, all samples exhibit the typical nanosheet structure of graphene. HRTEM characterization further indicates that these nanosheets consist of 1−10 layer graphenes. The interlayer distance is averagely ∼0.38 nm, slightly larger than the interlayer distance of graphite (∼0.34 nm), as a result of the thermal expansion. It can be seen clearly from these HRTEM images that the interlayer distance of outer sheets is evidently larger than that of inner sheets, confirming the XRD results. The EDX patterns shows both C and O elements for the undoped graphene sample, and the NG-T samples represent N element in addition to C and O elements, indicating that N is doped into these graphene nanosheets. All samples show a strong copper signal originated from the used copper grid holder.

AFM is considered the most direct method of quantifying the degree of exfoliation to a single-layer graphene sheet level and, thus, was used to estimate the average layer number of these nanosheets. As shown in Figure 3 demonstrating the AFM images of the four samples and their randomly chosen height profiles, the undoped graphene contains nanosheets with a thickness of ∼3.0 nm, confirming the XRD results and leading to a conclusion that GO cannot be completely exfoliated to single-layer graphene under the conditions. A graphene sheet is atomical flat with a well-known van der Waals thickness of ∼0.38 nm indicated by the above-reported HRTEM results.

dx.doi.org/10.1021/cs3000396 | ACS Catal. 2012, 2, 622−631

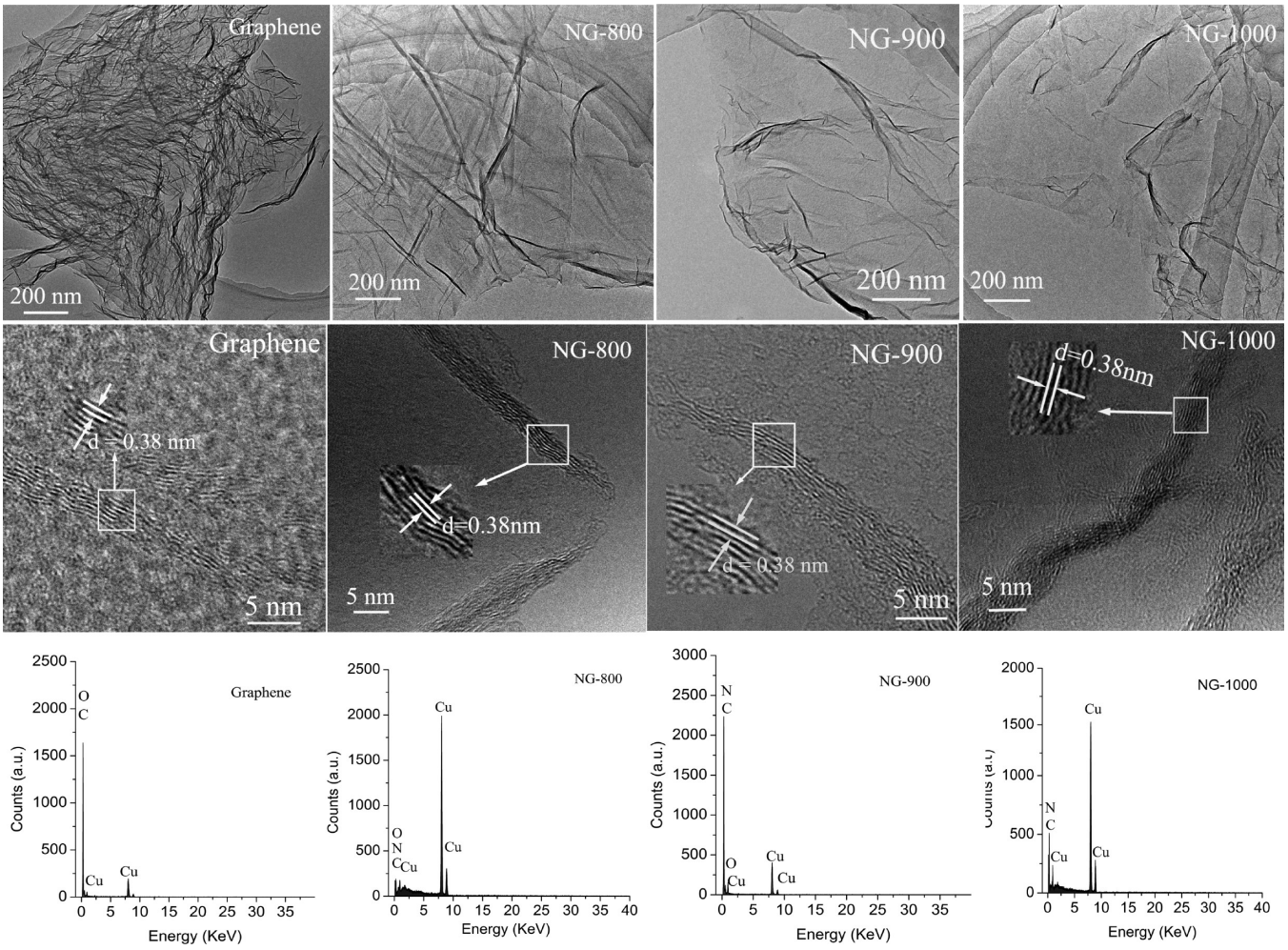

Figure 2. TEM and HRTEM images and EDX patterns of the NG-T and graphene samples.

The average layer number of the graphene nanosheets can be estimated to be ~8. For the three NG-T samples, the reactive NH_3 atmosphere has a negligible effect on the degree of high-temperature exfoliation of GO. The determined thickness of N-doped graphene nanosheets is between 2.9 to 3.2 nm, corresponding to a layer number of 8−9, which is consistent with that of graphene nanosheets. These AFM results are in good agreement with the above TEM results.

Raman spectroscopy is a powerful tool for identifying carbon materials and detecting the doping effect of graphene. Figure 4 compares the Raman spectra of NG-800, NG-900, NG-1000, and graphene. All samples display one intense D band at ~1310 cm^{-1} and one relatively weak G band at ~1597 cm^{-1}, without the 2D band of graphite at 2630 cm^{-1} (see Figure S2 in Supporting Information). This is consistent with the results of Gong.[44] It was well-known that the D band is a signature for disorder-induced vibrational mode. It is attributed to structural defects on the graphitic planes. The G band is commonly observed for all graphitic structures and assigned to the E_{2g} vibrational mode present in the sp^2 bonded graphitic carbons.

The intensity ratio of the former to the latter, namely, the I_D/I_G ratio, is an indication of the number of structural defects and a quantitative measure of edge plane exposure.[64] The disappearance of the 2D peak results from structural disorder and damaging of the lattice. Interestingly, the graphene obtained by annealing of GO in a He atmosphere exhibits an average value of I_D/I_G ratio (~1.56), comparable to that of the NG-800 (1.58) and NG-900 (1.51) samples, less than that (1.77) of the NG-1000 sample. This result offers us two aspects of information: One is that the high-temperature annealing in an inert atmosphere can create a large number of structural defects on graphitic planes by exfoliation of GO. Partial N heteroatoms may be introduced on these structural defect sites to form substitutional N species during nitridation. Another is that the formation of defects is with respect to annealing temperature, independent of nitridation. Annealing above 1273 K can produce larger numbers of structural defects.

Chemical States of N Species Doped in Multilayer Graphene. The chemical states of these N species doped into the flat lattice of graphene were characterized in detail by XPS. XPS spectra of N1s, C1s, and O1s obtained are shown in Figure 5. The atomic content of C, N, and O elements in these samples calculated from XPS spectra is summarized in Table 1. GO was annealed in He atmosphere at 1073 K, and the obtained graphene nanosheets show a weak O1s signal and no N1s signal in the XPS spectrum (Figure. 5A). After reaction with ammonia at a temperature range of 1073−1273 K, a weak N1s signal could be discerned from the XPS spectra, in addition to the O1s signal, indicating the incorporation of N atoms. It is estimated roughly from the intensity of the N1s signal that the content of te N species may decrease in the order NG-800 > NG-900 > NG-1000.

dx.doi.org/10.1021/cs3000396 | ACS Catal. 2012, 2, 622−631

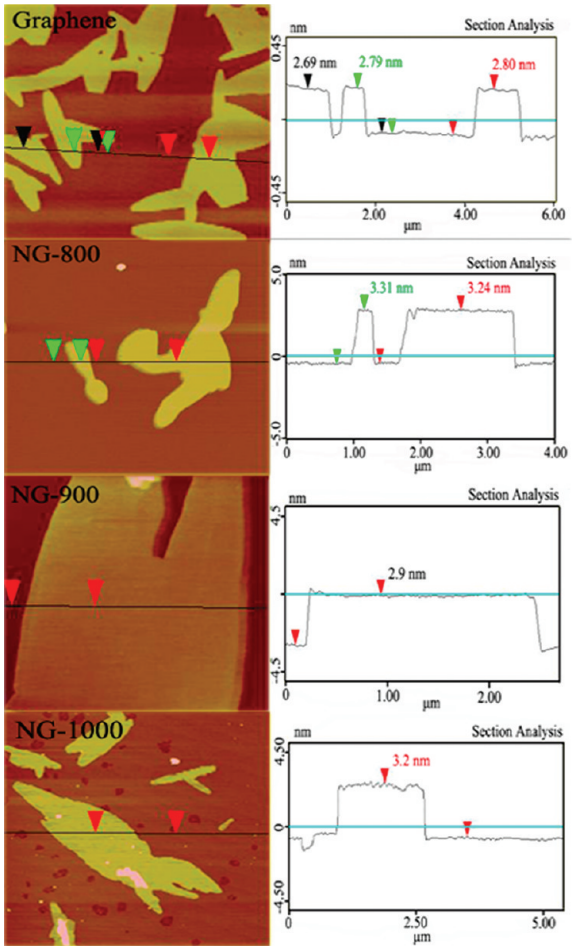

Figure 3. AFM images (left) and height profiles (right) of the NG-T and graphene samples.

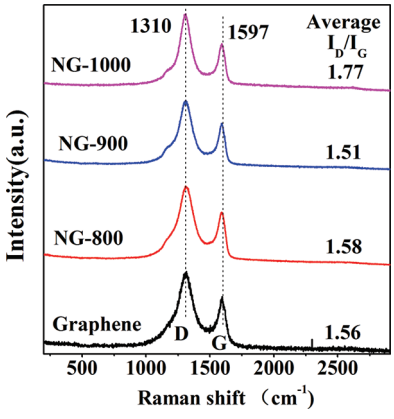

Figure 4. Visible−Raman spectra of the as-made NG-T and graphene samples.

The bonding configurations of N and O atoms in these N-doped multilayer graphenes were further studied on the basis of high-resolution XPS spectra. As shown in Figure 5B, the N1s peaks in the high-resolution XPS spectra of the NG-800, -900, and -1000 samples can be fitted into three peaks centered at 398.1 ± 0.1, 399.4, and 401.7 ± 0.1 eV, indicating that there are three types of N species present in these NG nanosheets. According to the literature,[6,44,65−67] the binding energy of 398.1 eV is attributed to pyridinic N (N_1), and the binding energy of 399.4 eV is ascribed to pyrrolic N (N_2). The peak at 401.7 eV

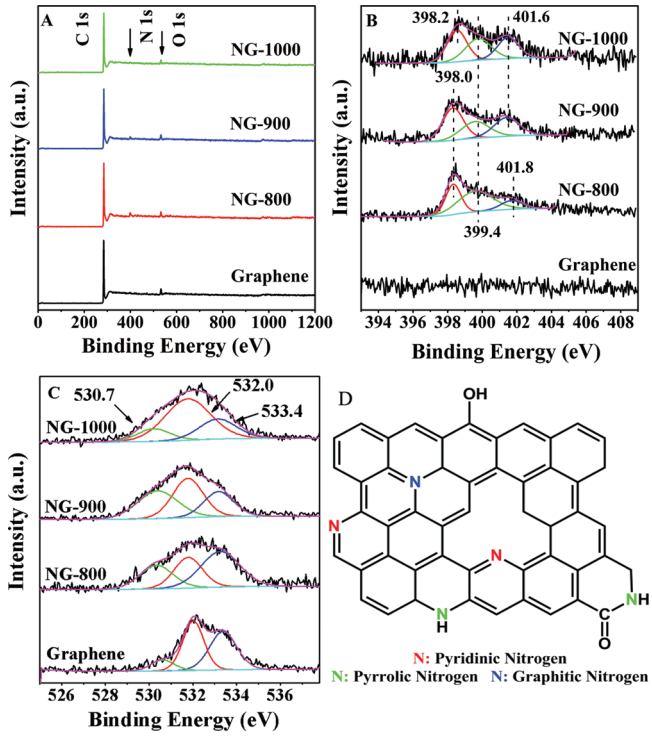

Figure 5. XPS spectra of the NG-T and graphene samples.

corresponds to graphitic N (N_3). Their molecular bonding structures are depicted clearly in Figure 5D. It can be seen from Table 1 that the N atomic content decreases monotonically from 4.16 to 1.71 at. % with an increase in the annealing temperature from 1073 to 1273 K, and pyridinic, and pyrrolic N species (N_1 + N_2) are predominant in these NG-T samples. It is important to note that a maximum content of 1.02 at. % for graphitic N species can be obtained upon reaction with ammonia at 1173 K, indicating an optimal temperature for the formation of N_3 species. Although the mechanism of N doping and the formation process of three types of N species remain unclear, it is unambiguous that the destruction of oxygen functional groups and the bonding reconstruction are necessary to incorporate N atoms into the flat lattice of graphene.

A primary clue to understanding the formation of graphitic N can be found from the evolution of N species with annealing temperature. As listed in Table 1, with increasing temperature from 1073 to 1173 K, the N_2 content decreases from 2.18 from NG-800 to 1.02 at. % from NG-900 along with the increase in the N_3 content from 0.57 for NG-800 to 1.02 at. % for NG-900, and the N_1 content keeps almost a constant value of 1.4 at. %. It suggests that N_3 maybe originate from N_2, which probably undergoes a condensation reaction of $=N^+-H + \equiv C-OH \rightarrow =N^+-C\equiv + H_2O$ at high temperature.[68] As such, annealing above 1173 K can also make C−N bonds break, leading to removal of the N dopant and formation of larger numbers of structural defects, as indicated by the aforementioned Raman results of NG-1000. This is consistent with the results reported in the literature.[49]

Figure 5C displays the high-resolution O1s XPS spectra of the NG-800, -900, and -1000 samples and the graphene sample. The broad O1s peak can be divided into three peaks centered at 530.6 ± 0.1, 532.2 ± 0.1, and 533.3 ± 0.1 eV. According to the literature,[67,69] the two subpeaks at 530.6 and 533.3 eV belong to C=O and ≡C−OH groups, respectively. However,

dx.doi.org/10.1021/cs3000396 | ACS Catal. 2012, 2, 622−631

Table 1. Distribution of Element Species Obtained from the De-Convolution of the C1s, N1s and O1s Peaks by XPS

		at. %			
entry	binding energy (eV)	graphene	NG-800	NG-900	NG-1000
total carbon (C)		96.1	92.4	92.7	95.1
total nitrogen (N)			4.16	3.48	1.71
pyridinic nitrogen (N_1)	398.0−398.2		1.41	1.44	0.65
pyrrolic nitrogen (N_2)	399.4−399.7		2.18	1.02	0.59
graphitic nitrogen (N_3)	401.3−401−6		0.57	1.02	0.47
total oxygen (O)		3.9	3.44	3.82	3.22
oxygen of C═O (O_1)	530.5−530.7	0.5	0.88	1.41	0.49
adsorbed oxygen (O_2)	532.0−532.3	1.7	0.98	1.51	1.95
oxygen of C−O (O_3)	533.2−533.4	1.7	1.58	0.90	0.78
N/C (at. %)			4.51	3.75	1.79
N_1/C (at. %)			1.53	1.55	0.68
N_2/C (at. %)			2.36	1.10	0.62
N_3/C (at. %)			0.62	1.10	0.49
O/C (at. %)		4.06	3.72	4.43	3.00
O_1/C (at. %)		0.52	0.95	1.52	0.52
O_2/C (at. %)		1.77	1.06	1.63	2.05
O_3/C (at. %)		1.77	1.71	0.98	0.83

Table 2. Catalytic Oxidation of Various Types of Alcohols over the NG-T and Graphene Samples[a]

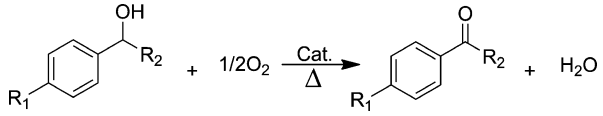

			reaction conditions				
entry	R_1	R_2	O_2 P (10^5 Pa)	T (K)	conversion (%)	selectivity (%)	yield (%)
1[b]	H	H	1.0	313			
2[b]	H	H	1.0	343			
3[c]	H	H	1.0	313	0.4	100	>99
4[c]	H	H	1.0	343	0.3	100	>99
5	H	H	1.0	313	3.5	100	>99
6	H	H	1.0	343	12.8	100	>98
7	NO_2	H	1.0	313	4.2	100	>99
8	NO_2	H	1.0	343	13.4	>95	>98
9	F	H	1.0	313	4.4	100	>99
10	F	H	1.0	343	15.9	100	>98
11	CH_3O	H	1.0	313	3.2	100	>99
12	CH_3O	H	1.0	343	14.8	100	>98
13	CH_3	H	1.0	313	3.0	100	>99
14	CH_3	H	1.0	343	10.6	>98	>98
15	H	CH_3	1.0	313	0.5	100	>99
16	H	CH_3	1.0	343	1.8	>98	>98
17[d]	H	H	1.0	343	6.1	100	>98
18[e]	H	H	1.0	343	6.5	100	>98
19[f]	H	H	1.0	343	4.0	100	>98

[a]Reaction conditions: 30 mg of NG900; 0.1 mmol of alcohol dissolved in 80 mL of H_2O; stirring speed, 1300 rpm; reaction time, 10 h. [b]No catalyst. [c]Graphene nanosheets. [d]N-doped MWCNTs (for preparation information, please refer to the Supporting Information). [e]NG-800. Reaction time: 3 h; yield (%) = $C_{BAD}/\Delta C_{BA} \times 100\%$, where BAD and BA are the abbreviations of benzaldehyde and benzylic alcohols, respectively. [f]NG-1000. Reaction time: 3 h; yield (%) = $C_{BAD}/\Delta C_{BA} \times 100\%$, where BAD and BA are the abbreviations of benzaldehyde and benzylic alcohols, respectively.

the assignment of the binding energy of 532.2 eV seems to be not straightforward. It may be contributed from both adsorbed oxygen and a minor amount of C−OH in −COOH groups for the graphene sample.[70−72] But for the three NG-T samples, it is believed that the subpeak at 532.2 eV belongs only to the adsorbed oxygen, because C−OH in residual −COOH groups can be consumed completely by the acid−base reaction of $-COOH + NH_3 \rightarrow O{=}C{-}NH_2 + H_2O$ at high temperature. As seen from Table 1, the content of the adsorbed O species in the NG-T samples increases monotonically with annealing temperature. This change is related to both the average I_D/I_G ratio obtained in Raman spectra, which is an indication of the number of structural defects, and the content of the graphatic N species. This suggests that O_2 molecules could be adsorbed on defects and N3 sites.

Catalytic Behavior for Aerobic Selective Oxidation of Primary Alcohols. The above-reported characterization results clearly indicate that N heteroatoms are incorporated

dx.doi.org/10.1021/cs3000396 | ACS Catal. 2012, 2, 622−631

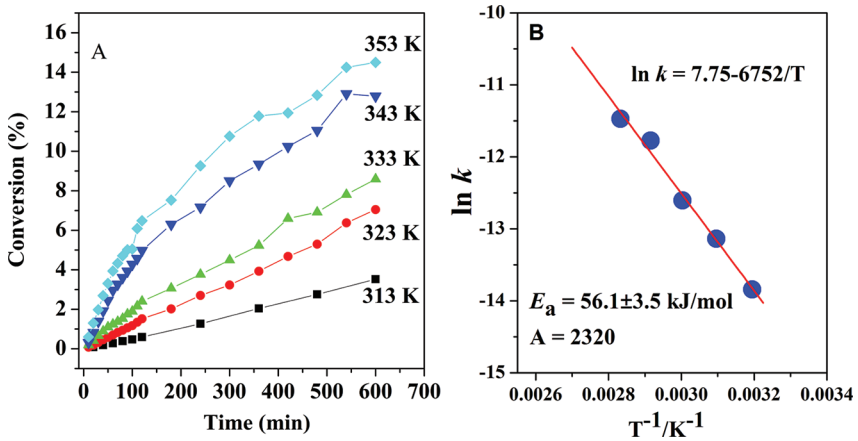

Figure 6. (A) Benzyl alcohol conversion profiles obtained at the indicated reaction temperature using NG-900 catalyst. (B) Arrhenius plot of the oxidation of benzyl alcohol with molecular oxygen.

into the flat lattice of multilayer graphene nanosheets as pyridinic, pyrrolic, and quaternary N complexes by the postnitridation. Much study[44,73] has shown that the doping of N species can transform the p-type graphene into n-type graphene. Consequently, the intrinsic change in electron structure of graphene will bring about some unique chemical properties.

In this study, we explore systematically a novel application of N-doped multilayer graphene in aerobic selective oxidation of primary alcohols in water. We chose six types of alcohols as reactive substrates to fully evaluate the selectively catalytic performance of these NG-T samples under mild conditions. A special emphasis was placed on the oxidation of benzyl alcohol to benzaldehyde to better understand the nature of nonmetal catalysis for the aerobic oxidation of alcohols.

The NG-900 sample was used as a representative catalyst to study in detail the selective oxidation. Table 2 lists the activity results obtained with a range of substrates and reaction conditions. In two control experiments without catalyst, which were conducted at 313 and 343 K, no products derived from oxidation of the substrate are detected by HPLC. In two reference experiments with the undoped graphene sample as catalyst, a negligible amount (0.3−0.4%) of benzyl alcohol is selectively oxidzed to benzaldehyde within a reaction time of 10 h, independent of reaction temperature, suggesting that the conversion over the undoped graphene nanosheets is not a catalytic process, but originates from the oxidation of defects or reactive O or carbene groups left at the edges and corners of the graphene nanosheets.[74] The introduction of N heteroatoms into the flat lattice of graphene nanosheets enhances greatly the benzyl alcohol conversion to 4.00% at 313 K and 12.8% at 343 K under the same conditions and keeps 100% selectivity to aldehyde. For the oxidation of other primary alcohols, including *p*-nitrobenzyl alcohol, *p*-fluorobenzyl alcohol, *p*-methyl benzyl alcohol, and *p*-methoxybenzyl alcohol, the NG-900 catalyst also exhibits a ∼4-fold enhancement upon increasing the reaction temperature from 313 to 343 K, indicating that the N-doped graphene materials have a commonality in the catalytic aerobic oxidation of primary alcohols. Moreover, we note that the NG-900 catalyst seems to be catalytically inactive for secondary alcohols, as indicated by a very low conversion of 1.8% for 1-phenyl ethyl alcohol at 343 K. This is probably due to the spatial confinement.

To reveal the origin and activity of N-doped graphene for the aerobic oxidation of primary alcohols to the corresponding aldehydes, the kinetic analysis for catalytic oxidation is necessary. Here, the oxidation of benzyl alcohol to benzaldehyde was used as a model reaction to obtain some pivotal kinetic parameters. Figure 6A shows the benzyl alcohol conversion as a function of reaction temperature. The results were obtained at a high stirring speed of 1300 rpm, where the reaction already escaped the mass-transfer-controlled regime into a kinetic control regime independent of stirring. It appears that as the reaction temperature increases from 313 to 353 K, the benzyl alcohol conversion increases gradually from 3.5% to 14.5% after a reaction time of 10 h, but the selectivity slightly decreases above 343 K. A minor amount of benzoic acid could be detected at 353 K, indicating the occurrence of deep oxidation at such a temperature.

Considering the selectivity, the optimal temperature that may be usable for analysis of the reaction kinetics is between 313 to 353 K. According to the Arrhenius equation of $\ln k = \ln A - E_a/RT$, we plotted $\ln k$ versus $1/T$, where k is the rate constant obtained by linearly fitting the conversion curve of benzyl alcohol within the initial 60 min of the reaction at an indicated temperature. The plot of $\ln k$ versus $1/T$ is satisfactorily linear, as shown in Figure 6B. The slope and intercept are −6752 and 7.75, respectively, from which the apparent activation energy (E_a) and pre-exponential factor (A) calculated by the Arrhenius equation are 56.1 ± 3.5 kJ·mol^{-1} and 2.32 × 10^3 mol^{-1}·dm^3·s^{-1}, respectively. The moderate activation energy (E_a) is very close to that (51.4 kJ·mol^{-1}) reported for Ru/Al_2O_3-catalyzed aerobic benzyl alcohol oxidation using $PhCF_3$ as solvent.[75] From the kinetic data, the reaction rate (R) can be expressed as follows (eq 1):

$$R = -\mathrm{d}[\text{benzyl alcohol}]/\mathrm{d}t = k_{obs}[\text{catalyst}]^1[\text{benzyl alcohol}]^{\alpha}[O_2]^{\beta}$$

where

$$k_{obs} = 2.32 \times 10^3 \exp(-6.75 \times 10^3/T) \quad (1)$$

The reaction orders on these N-doped graphene catalysts were determined by considering eq 1. The α values were determined by varying the benzyl alcohol concentration between 0.3 and 2.4 mmol·L^{-1} at a fixed O_2 partial pressure (1.0 atm). Similarly, reaction order β was obtained by varying

dx.doi.org/10.1021/cs3000396 | ACS Catal. 2012, 2, 622−631

the partial pressure of O_2 (P_{O_2}) between 0.4 and 1.0 atm while keeping the benzyl alcohol concentration (C_{BA}) at 1.2 mmol·L^{-1}. In Figure 7, the r values obtained on the N-doped

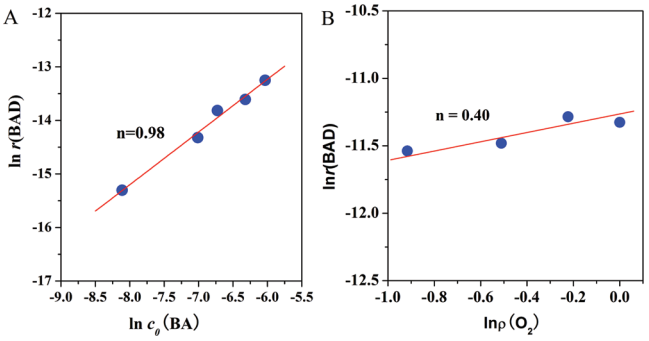

Figure 7. (A) Dependence of benzyl alcohol oxidation reaction upon the alcohol concentration. Catalyst, 30 mg of NC-900; O_2 partial pressure, 1.0 atm. (B) Dependence of benzyl alcohol oxidation reaction upon oxygen partial concentration. Catalyst, 30 mg of NC-900; reactant concentration, 1.2 mmol·L^{-1}.

graphene catalysts are represented in logarithmic plots as a function of C_{BAD} and P_{O_2}. Reaction orders α and β are determined graphically from Figure 7A and B to be 0.98 and 0.40, respectively. The obtained reaction orders α and β are close to their corresponding theoretical values, 1.0 and 0.5, indicating that the N-doped graphene-catalyzed aerobic alcohol oxidation is an atom-economic reaction. However, the representation of eq 1 cannot elucidate fully the reaction mechanism, and hence, further analysis and discussion is necessary below.

In general, a heterogeneous catalytic reaction proceeds by three possible mechanisms as follows: (i) the Eley–Rideal mechanism; (ii) the Langmuir–Hinshelwood model; (iii) the Mars–van Krevelen mechanism.[22] The Eley–Rideal mechanism requires one of the reactants to be in the gas phase, and the Mars–van Krevelen mechanism involves participation of the lattice oxygen of the catalyst in the catalytic network. However, here, the conversion of benzyl alcohol is basically invariant whether O_2 is bubbled through the slurry phase or just passed over the liquid surface (see Figure S3 in Supporting Information). This implies that mass transfer of oxygen to the liquid phase is not a rate-determining step, and the reacting species is dissolved oxygen. Moreover, the active component of the catalyst can be established to be N species, according to the characterization results above; hence, it can be concluded that the reaction mechanisms above noted as i and iii are not applicable. The classical Langmuir–Hinshelwood model involves adsorption of reactants (benzyl alcohol and oxygen) on active sites at the surface, followed by an irreversible rate-determining surface reaction to give products. The following rate expression is obtained by the L–H rate law:

$$R = \frac{kK_1k_2[\mathrm{PhCH_2OH}][\mathrm{O_2}]^{0.5}}{[1 + K_1[\mathrm{PhCH_2OH}] + K_2[\mathrm{O_2}]^{0.5}]^2} \quad (2)$$

where k is the rate constant for the surface reaction and K_1 and K_2 are the adsorption constants of $PhCH_2OH$ and O_2, respectively. If both $PhCH_2OH$ and O_2 molecules have very low adsorption on active sites, together with the low concentrations of $PhCH_2OH$ and oxygen dissolved in water (0.0569 mmol·L^{-1}, at 1.0 atm oxygen and 343 K), that is, $K_1[\mathrm{PhCH_2OH}]$ and $K_2[\mathrm{O_2}] \ll 1$, eq 2 can be simplified to the following rate expression [eq 3].

$$R \cong kK_1K_2[\mathrm{PhCH_2OH}][\mathrm{O_2}]^{0.5} \quad (3)$$

Equation 3 is basically equivalent to eq 1 obtained above. This suggests that the L–H mechanism is most likely occurring in the oxidation of benzyl alcohol over N-doped graphene. The weak adsorption of reactants ($PhCH_2OH$ and O_2) on active sites is well verified by the lowest A value of 2.32×10^3, which is 3 orders of magnitude smaller than that (3.44×10^6) taking place on the catalyst Ru/Al_2O_3 using $PhCF_3$ as solvent.[75]

Proposed Reaction Mechanism for N-Graphene Catalyzed Aerobic Alcohol Oxidation. To clarify the noncatalytic conversion of benzyl alcohol over graphene, we first detected the intermediates formed during reaction by a spin-trapping electron paramagnetic resonance (EPR) technique using 5,5-dimethyl-1-pyrroline N-oxide (DMPO) as the spin trap. As shown in Figure 8A, these sextet peaks are the

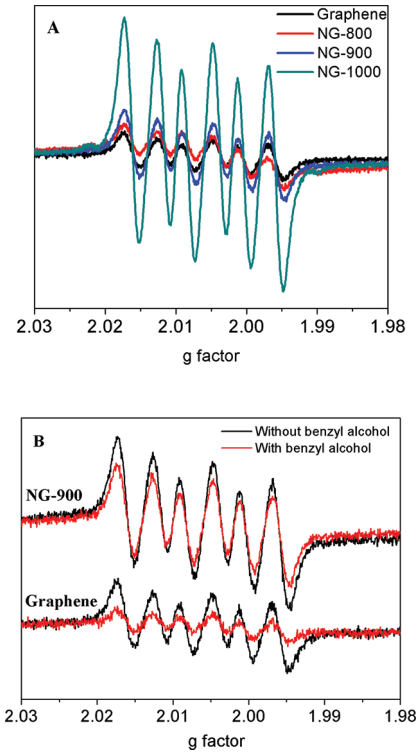

Figure 8. (A) EPR spectra of TEMPO-OCH_3 adduct over NG-T and graphene catalysts.

typical EPR signatures of DMPO–·OCH_3 adducts;[76] no other signals originating from species such as DMPO–·OH, DEMPO–$O_2^{\bullet-}$, and DMPO–·CH_2OH adducts appear. This shows that these NG-T and graphene samples prepared by the high temperature exfoliation method can react directly with methanol to produce the methoxy radical, independent of N dopant. It indicates that the formation of ·OCH_3 is correlated closely with electron-deficient defects emerging on the surface. Moreover, it appears that the intensity of the EPR lines decreases in the order of NG-1000 > NG-800 ≈ graphene, in line with their average I_D/I_G ratio obtained in the Raman spectra. This further confirms the aforementioned conclusion.

It is interesting to note that NG-900 with the fewest defects shows a greater amount of DMPO–·OCH_3 compared with

dx.doi.org/10.1021/cs3000396 | ACS Catal. 2012, 2, 622–631

NG-800 and graphene, suggesting that one among the three types of N species is able to activate methanol to form the methoxy radical. After adding benzyl alcohol, the EPR line intensity decreases immediately and stays constant for both NG-900 and graphene, as shown in Figure 8B. This suggests that benzyl alcohol may be activated by the electron-deficient defects and the N dopant to form the $C_6H_5CH_2O\cdot$ radical, which competes with $\cdot OCH_3$, consequently causing the decrease in the DMPO−$\cdot OCH_3$ adducts. Therefore, it is reasonable to deduce that the minor amount of product benzaldehyde obtained may be derived from the noncatalytic oxidation of benzyl alcohol by the electron-deficient defects emerging on the graphene flat. Considering that the activity results following the decreasing order of NG-900 > NG-800 > NG-1000 (Figure S4 of the Supporting Information), we are sure that the aerobic alcohol oxidation taking place on the NG-T samples originates predominantly from the catalysis of the N dopant. It can be thus concluded that the N dopant is the catalytically active component, instead of C and O elements, whereas the noncatalytic contribution from these defects, including reactive edges, corners, and carbene, cannot be excluded completely for the alcohol oxidation reaction.[60]

The aforementioned XPS results show that the postnitration for multilayer graphene results in the formation of three types of N species: pyridinic N (N_1), pyrrolic N (N_2), and graphitic N (N_3). Which one is the catalytically active species? According to the atomic content obtained from XPS spectra for N species, we plotted the N/C atomic ratio versus the initial reaction rate. As shown in Figure 9, a good linear relationship is found

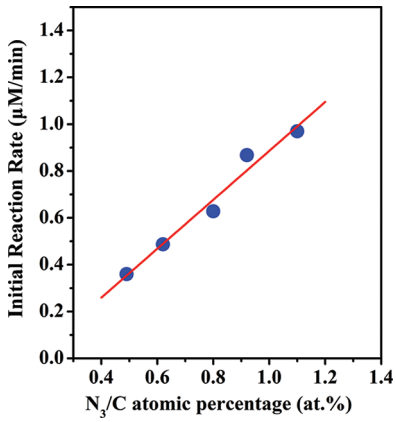

Figure 9. Relationship between initial reaction rate and graphitic N species.

between the N_3/C atomic ratio and the initial reaction rate, but for the other two kinds of species, N_1 and N_2, no correlation with the activity results can be established. It suggests that the graphitic sp^2 N species are closely correlated with the aerobic catalytic oxidation. The aforementioned kinetic analysis reveals that the aerobic alcohol oxidation reaction catalyzed by N-doped graphene follows a L−H mechanism. Thus, we can demonstrate a general picture of the oxidation reaction process as displayed in Scheme 1.

The adsorption and activation of molecular oxygen over the graphitic N active sites to form a sp^2 N−O_2 adduct transition state may be a key element step. The activated oxygen shows high chemical reactivity to primary alcohols, possibly because it directly attacks the α-H atom of alcohol to finally form water. This can well explain the formation of the larger number of

Scheme 1. Proposed Reaction Pathway for Aerobic Alcohol Oxidation over N-Doped Graphene Nanosheets

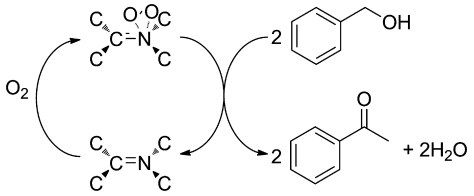

methoxy radicals over the NG-900 catalyst. No H_2O_2 during the catalytic reaction was detected, as shown by Figure S5 (see the Supporting Information), indirectly verifying the assumption. Secondary alcohols, such as 1-phenyl ethyl alcohol, commonly present a low conversion due to the steric interference from the methyl group as the electron donor. The spatial selectivity in the reactive domain may be one of the important parameters determining the pre-exponential factor value of N-doped multilayer graphene catalysts.

CONCLUSIONS

In summary, N doping unexpectedly creates a new chemical function for graphene nanosheets. Green, efficient, aerobic oxidation of primary alcohols to corresponding aldehydes can proceed over metal-free, N-doped graphene nanosheets under mild conditions. The detailed surface analysis for a series of samples prepared at different temperatures discloses the structural−performance relationship of the N-doped graphene materials and demonstrates that the metal-free catalysis takes place on the graphitic sp^2 nitrogen sites. The detailed kinetic analysis clearly reveals a Langmuir−Hinshelwood pathway for the graphitic sp^2 nitrogen-catalyzed aerobic alcohol oxidation. It has a moderate overall activation energy of 56.1 ± 3.5 kJ·mol^{-1} and a very low pre-exponential factor of 2.32 × 10^3, which is one of the important parameters affecting the unsatisfactory conversion. No other active oxygen species, such as $O_2^{-\bullet}$, $\cdot OH$, or H_2O_2 that were often found in the noble metal-catalyzed system, are determined using EPR spin trapping technique and photometric method, suggesting that the reaction may involve the formation of a sp^2 N−O_2 adduct transition state that has a high chemical reactivity to alcohols. The EPR characterization results definitely elucidate the noncatalytic conversion of alcohols to aldhydes over graphene, which was contributed mainly from the reaction of carbene or electron-deficient defects with reactant alcohol.

EXPERIMENTAL SECTION

Chemical reagents used for the preparation of samples include graphite powder, NaCl, concentrated H_2SO_4, $NaNO_3$, $KMnO_7$, H_2O_2, and HCl. They were all purchased from Sinopharm Chemical Reagent Co., Ltd. All these chemicals were of analytical grade purity and were used without further purification. Ammonia gas, supplied by Fuzhou Xinhang Industrial Gases Co., Ltd., was industrial grade (>95%).

Synthesis of Graphene and Nitrogen-Doped Graphene Nanosheets. For the catalyst preparation, GO was first made via a modified Hummers method.[62] To produce nitrogen-doped graphene nanosheets, a heat-treatment procedure of the as-synthesized GO at different temperatures under ammonia flow (300 mL·min^{-1}) was applied. The details of this procedure are described as follows. GO samples were placed into an Al_2O_3 boat in the center of a tube furnace. After flowing

dx.doi.org/10.1021/cs3000396 | ACS Catal. 2012, 2, 622−631

with NH_3 for 30 min, the temperature of the furnace was raised to 573 K in 15 min and then directly heated to the indicated reaction temperature at a heating rate of 5 K·min^{-1}. Three nitridation temperatures of 1073, 1173, and 1273 K were chosen to obtain samples with different nitrogen concentrations. After 10 h of calcination at an indicated temperature, the furnace was cooled down naturally to room temperature. To completely remove the ammonia adsorbed on the surface of the samples, the furnace was flowed with a He stream for more than 30 min after nitridation. The obtained products were designated as NG-T (T = 800, 900, and 1000), respectively. For comparison, graphene nanosheets were synthesized by heating GO at 1073 K under flowing He.

Catalyst Characterizations. X-ray powder diffraction patterns were recorded on a Bruker D8 Advance X-ray diffractometer using Cu Kα1 radiation (λ = 1.5406 Å), 40 kV, and 40 mA with a scanning speed of 0.2° (2θ) min^{-1}. Transmission electron microscopy images were collected on a JEOL model JEM 2010 EX microscope at an accelerating voltage of 200 kV. The XPS spectra were carried out on an ESCALAB 250 XPS system with a monochromatized Al Ka X-ray source (15 kV, 200 W, 500 μm, pass energy = 20 eV). Tapping-mode AFM measurements were performed on a Nanoscope IIIA system. Samples for AFM imaging were prepared by depositing suspensions of NG-T on freshly cleaved mica surfaces. The Raman spectra were measured using a laser with an excitation wavelength of 785 nm at room temperature on a Renishaw Raman microscope. EPR spectra were recorded by a Bruker A-300-EPR X-band spectrometer at room temperature. Typically, the methanol solution of DMPO was added to the samples (5 mg), and then the mixture was sampled using a capillary tube and placed in a EPR tube for EPR experiments.

Catalytic Activity Testing. The oxidation reactions were carried out in a flask containing 80 mL of deionized water, 0.1 mmol of alcohol, 30 mg of catalyst, and a stir bar. Unless otherwise indicated, the aerobic oxidation reactions were conducted in an oil bath at 343 K in a static O_2 atmosphere (1.0 atm). The reaction solution was sampled periodically and analyzed and quantified by liquid chromatography (Waters 2487) equipped with a Agilent Zorbax SB-C18 column. Kinetic measurements were conducted at a temperature range of 313−343 K. The conversion of alcohol was controlled below 5.0% to collect data.

■ ASSOCIATED CONTENT

Ⓢ Supporting Information

XRD patterns of graphite and graphite oxide; Raman spectrum of graphite as well as the statistics of the I_D/I_G value for different samples; conversion of benzyl alcohol in static O_2 atmosphere and under bubbling O_2; conversion of benzyl alcohol over NG-T catalysts at 343 K for 1.5 h; experimental details of the detection of H_2O_2; preparation of nitrogen-doped MWCNTs. This material is available free of charge via the Internet at http://pubs.acs.org/.

■ AUTHOR INFORMATION

Corresponding Author

*Phone: +86-591-83779121. Fax: +86-591-83779251. E-mail: (J.L.) jllong@fzu.edu.cn, (X.W.) xwang@fzu.edu.cn.

Notes

The authors declare no competing financial interest.

■ ACKNOWLEDGMENTS

This work was financially supported by the NSFC (Grants Nos. 21003021 and 21173044), the Natural Science Foundation of Fujian Province of P. R. China (2010J05024), the Science and Technology Project of Education Office of Fujian Province of P. R. China (JK2010002), and the National Basic Research Program of China (973 Program, No. 2012CB722607 and 2011CB612314). We also express our gratitude to Ms. Pan Danmei, from Fujian Institute of Research on the Structure of Matter, Chinese Academy of Sciences, for her assistance with the AFM analysis.

■ REFERENCES

(1) Brink, G.-J. T.; Arends, I. W. C. E.; Sheldon, R. A. *Science* **2000**, *287*, 1636−1639.
(2) Sheldon, R. A.; Arends, I. W. C. E.; Brink, G.-J. T.; Dijksman, A. *Acc. Chem. Res.* **2002**, *35*, 774−781.
(3) Sheldon, R. A.; Arends, I. W. C. E.; Dijksman, A. *Catal. Today* **2000**, *57*, 157−166.
(4) Ansari, I. A.; Gree, R. *Org. Lett.* **2002**, *4*, 1507−1509.
(5) Zhan, B.-Z.; Thompson, A. *Tetrahedron* **2004**, *60*, 2917−2935.
(6) Schultz, M. J.; Sigman, M. S. *Tetrahedron* **2006**, *62*, 8227−8241.
(7) Gamez, P.; Arends, I. W. C. E.; Sheldon, R. A.; Reedijk, J. *Adv. Synth. Catal.* **2004**, *346*, 805−811.
(8) Wu, G.; Wang, X.; Li, J.; Zhao, N.; Wei, W.; Sun, Y. *Catal. Today* **2008**, *131*, 402−407.
(9) Lebeau, E. L.; Meyer, T. J. *Inorg. Chem.* **1999**, *38*, 2174−2181.
(10) Chaudhuri, P.; Hess, M.; Weyhermüller, T.; Wieghardt, K. *Angew. Chem., Int. Ed.* **1999**, *38*, 1095−1098.
(11) Cainelli, G.; Cardillo, G. *Chromium Oxidations in Organic Chemistry*; Springer: Berlin, 1984; pp 118−216.
(12) Mallat, T.; Baiker, A. *Chem. Rev.* **2004**, *104*, 3037−3058.
(13) Besson, M.; Gallezot, P. *Catal. Today* **2000**, *57*, 127−141.
(14) Choudhary, V. R.; Chaudhari, P. A.; Narkhede, V. S. *Catal. Commun.* **2003**, *4*, 171−175.
(15) Liu, R.; Dong, C.; Liang, X.; Wang, X.; Hu, X. *J. Org. Chem.* **2005**, *70*, 729−731.
(16) Liu, R.; Liang, X.; Dong, C.; Hu, X. *J. Am. Chem. Soc.* **2004**, *126*, 4112−4113.
(17) Shibuya, M.; Osada, Y.; Sasano, Y.; Tomizawa, M.; Iwabuchi, Y. *J. Am. Chem. Soc.* **2011**, *133*, 6497−6500.
(18) Shibuya, M.; Tomizawa, M.; Suzuki, I.; Iwabuchi, Y. *J. Am. Chem. Soc.* **2006**, *128*, 8412−8413.
(19) Hoover, J. M.; Stahl, S. S. *J. Am. Chem. Soc.* **2011**, *133*, 16901−16910.
(20) Jensen, D. R.; Schultz, M. J.; Mueller, J. A.; Sigman, M. S. *Angew. Chem.* **2003**, *115*, 3940−3943.
(21) Markó, I. E.; Gautier, A.; Dumeunier, R.; Doda, K.; Philippart, F.; Brown, S. M.; Urch, C. J. *Angew. Chem., Int. Ed.* **2004**, *43*, 1588−1591.
(22) Makwana, V. D.; Son, Y.-C.; Howell, A. R.; Suib, S. L. *J. Catal.* **2002**, *210*, 46−52.
(23) Son, Y.-C.; Makwana, V. D.; Howell, A. R.; Suib, S. L. *Angew. Chem., Int. Ed.* **2001**, *40*, 4280−4283.
(24) Yamaguchi, K.; Mizuno, N. *Angew. Chem.* **2002**, *114*, 4720−4724.
(25) Zhan, B.-Z.; White, M. A.; Sham, T.-K.; Pincock, J. A.; Doucet, R. J.; Rao, K. V. R.; Robertson, N.; Cameron, T. S. *J. Am. Chem. Soc.* **2003**, *125*, 2195−2199.
(26) Miyamura, H.; Matsubara, R.; Miyazaki, Y.; Kobayashi, S. *Angew. Chem.* **2007**, *119*, 4229−4232.
(27) Choudhary, V. R.; Dhar, A.; Jana, P.; Jha, R.; Uphade, B. S. *Green Chem.* **2005**, *7*, 768−770.
(28) Choudhary, V. R.; Jha, R.; Jana, P. *Green Chem.* **2007**, *9*, 267−272.
(29) Mori, K.; Hara, T.; Mizugaki, T.; Ebitani, K.; Kaneda, K. *J. Am. Chem. Soc.* **2004**, *126*, 10657−10666.

(30) Yamada, Y. M. A.; Arakawa, T.; Hocke, H.; Uozumi, Y. *Angew. Chem.* **2007**, *119*, 718−720.
(31) Tsunoyama, H.; Sakurai, H.; Negishi, Y.; Tsukud, T. *J. Am. Chem. Soc.* **2005**, *127*, 9374−9375.
(32) Yuan, Y.; Yan, N.; Dyso, P. J. *Inorg. Chem.* **2011**, *50*, 11069−11074.
(33) Su, F.-Z.; Liu, Y.-M.; Wang, L.-C.; Cao, Y.; He, H.-Y.; Fan, K.-N. *Angew. Chem.* **2008**, *120*, 340−343.
(34) Enache, D. I.; Edwards, J. K.; Landon, P.; Solsona-Espriu, B.; Carley, A. F.; Herzing, A. A.; Watanabe, M.; Kiely, C. J.; Knight, D. W.; Hutching, G. J. *Science* **2006**, *311*, 362−365.
(35) Hou, W.; Dehm, N. A.; Scott, R. W. J. *J. Catal.* **2008**, *253*, 22−27.
(36) Sheldon, R. A.; Arends, I. W. C. E. *Adv. Synth. Catal.* **2004**, *346*, 1051−1071.
(37) Gilhespy, M.; Lok, M.; Baucherel, X. *Catal. Today* **2006**, *117*, 114−119.
(38) Brunel, D.; Fajula, F.; Nagy, J. B.; Deroide, B.; Verhoef, M. J.; Veum, L.; Peters, J. A.; van Bekkum, H. *Appl. Catal., A* **2001**, *213*, 73−82.
(39) Pozzi, G.; Cavazzini, M.; Quici, S.; Benaglia, M.; Dell'Anna, G. *Org. Lett.* **2004**, *6*, 441−443.
(40) Fey, T.; Fischer, H.; Bachmann, S.; Albert, K.; Bolm, C. *J. Org. Chem.* **2001**, *66*, 8154−8159.
(41) Karimi, B.; Badreh, E. *Org. Biomol. Chem.* **2011**, *9*, 4194−4198.
(42) Wei, D.; Liu, Y.; Wang, Y.; Zhang, H.; Huang, L.; Yu, G. *Nano Lett.* **2009**, *9*, 1752−1758.
(43) Geng, D.; Yang, S.; Zhang, Y.; Yang, J.; Liu, J.; Li, R.; Sham, T.-K.; Sun, X.; Ye, S.; Knights, S. *Appl. Surf. Sci.* **2011**, *257*, 9193−9198.
(44) Guo, B.; Liu, Q.; Chen, E.; Zhu, H.; Fang, L.; Gong, J. R. *Nano Lett.* **2010**, *10*, 4975−4980.
(45) Zhao, L.; He, R.; Rim, K. T.; Schiros, T.; Kim, K. S.; Zhou, H.; Gutiérrez, C.; Chockalingam, S. P.; Arguello, C. J.; Pálová, L.; Nordlund, D.; Hybertsen, M. S.; Reichman, D. R.; Heinz, T. F.; Kim, P.; Pinczuk, A.; Flynn, G. W.; Pasupathy, A. N. *Science* **2011**, *333*, 999−1003.
(46) Luo, Z.; Lim, S.; Tian, Z.; Shang, J.; Lai, L.; MacDonald, B.; Fu, C.; Shen, Z.; Yu, T.; Lin, J. *J. Mater. Chem.* **2011**, *21*, 8038−8044.
(47) Sheng, Z.-H.; Shao, L.; Chen, J.-J.; Bao, W.-J.; Wang, F.-B.; Xia, X.-H. *ACS Nano* **2011**, *5*, 4350−4358.
(48) Qu, L.; Liu, Y.; Baek, J.-B.; Dai, L. *ACS Nano* **2010**, *4*, 1321−1326.
(49) Geng, D.; Chen, Y.; Chen, Y.; Li, Y.; Li, R.; Sun, X.; Ye, S.; Knights, S. *Energy Environ. Sci.* **2011**, *4*, 760−764.
(50) Deng, D.; Yu, L.; Pan, X.; Wang, S.; Chen, X.; Hu, P.; Sun, L.; Bao, X. *Chem. Commun.* **2011**, *47*, 10016−10018.
(51) Liu, X.; Frank, B.; Zhang, W.; Cotter, T. P.; Schögl, R.; Su, D. S. *Angew. Chem., Int. Ed.* **2011**, *50*, 3318−3322.
(52) Frank, B.; Zhang, J.; Blume, R.; Schögl, R.; Su, D. S. *Angew. Chem., Int. Ed.* **2009**, *48*, 6913−6917.
(53) Zhang, J.; Liu, X.; Blume, R.; Zhang, A.; Schögl, R.; Su, D. S. *Science* **2008**, *322*, 73−77.
(54) Dreyer, D. R.; Jia, H.-P.; Bielawski, C. W. *Angew. Chem., Int. Ed.* **2010**, *49*, 6813−6816.
(55) Dreyer, D. R.; Bielawski, C. W. *Chem. Sci.* **2011**, *2*, 1233−1240.
(56) Dreyer, D. R.; Ruoff, R. S.; Bielawski, C. W. *Angew. Chem., Int. Ed.* **2010**, *49*, 9336−9344.
(57) Jia, H.-P.; Dreyer, D. R.; Bielawski, C. W. *Adv. Synth. Catal.* **2011**, *353*, 528−532.
(58) Dreyer, D. R.; Jarvis, K. A.; Ferreira, P. J.; Bielawski, C. W. *Macromolecules* **2011**, *44*, 7659−7667.
(59) Dreyer, D. R.; Jia, H.-P.; Todd, A. D.; Geng, J.; Bielawski, C. W. *Org. Biomol. Chem.* **2011**, *9*, 7292−7295.
(60) Jia, H.-P.; Dreyer, D. R.; Bielawski, C. W. *Tetrahedron* **2011**, *67*, 4431−4434.
(61) Li, X.; Wang, H.; Robinson, J. T.; Sanchez, H.; Diankov, G.; Dai, H. *J. Am. Chem. Soc.* **2009**, *131*, 15939−15944.
(62) Hummers, W. S.; Offeman, R. E. *J. Am. Chem. Soc.* **1958**, *80*, 1339−1339.
(63) Rao, C. N. R.; Sood, A. K.; Subrahmanyam, K. S.; Govindaraj, A. *Angew. Chem., Int. Ed.* **2009**, *48*, 7752−7777.
(64) Luo, D.; Zhang, G.; Liu, J.; Sun, X. *J. Phys. Chem. C* **2011**, *115*, 11327−11335.
(65) Casanovas, J.; Ricart, J. M.; Rubio, J.; Illas, F.; Jiménez-Mateos, J. M. *J. Am. Chem. Soc.* **1996**, *118*, 8071−8076.
(66) Zhang, L.-S.; Liang, X.-Q.; Song, W.-G.; Wu, Z.-Y. *Phys. Chem. Chem. Phys.* **2010**, *12*, 12055−12059.
(67) Yang, D.; Velamakanni, A.; Bozoklu, G.; Park, S.; Stoller, M.; Piner, R. D.; Stankovich, S.; Jung, I.; Field, D. A.; Ventrice, C. A. Jr.; Ruoff, R. S. *Carbon* **2009**, *47*, 145−152.
(68) Saidi, O.; Blacker, A. J.; Farah, M. M.; Marsden, S. P.; Williams, J. M. J. *Chem. Commun.* **2010**, *46*, 1541−1543.
(69) Long, D.; Li, W.; Ling, L.; Miyawaki, J.; Mochida, I.; Yoon, S.-H. *Langmuir* **2010**, *26*, 16096−16102.
(70) Dupin, J.-C.; Gonbeau, D.; Vinatier, P.; Levasseur, A. *Phys. Chem. Chem. Phys.* **2000**, *2*, 1319−1324.
(71) Rao, C. N. R.; Kamath, P. V.; Yashonath, S. *Chem. Phys. Lett.* **1982**, *88*, 13−16.
(72) Bao, X.; Deng, J.; Dong, S. *Surf. Sci.* **1985**, *163* (2−3), 444−456.
(73) Wang, X.; Li, X.; Zhang, L.; Yoon, Y.; Weber, P. K.; Wang, H.; Guo, J.; Dai, H. *Science* **2009**, *324*, 768−771.
(74) Frank, B.; Blume, R.; Rinaldi, A.; Trunschke, A.; Schlögl, R. *Angew. Chem., Int. Ed.* **2011**, *50*, 10226−10230.
(75) Yamaguchi, K.; Mizuno, N. *Chem.—Eur. J.* **2003**, *9*, 4353−4361.
(76) Chen, F.; Xie, Y.; He, J.; Zhao, J. *J. Photochem. Photobiol. A: Chem.* **2001**, *138*, 139−146.